

Article

Pressure-Driven Sample Flow through an Electrospun Membrane Increases the Analyte Adsorption

Aitsana Maslakova ¹, Kirill Prusakov ^{1,2}, Anastasia Sidorova ¹, Elizaveta Pavlova ², Alla Ramonova ¹
and Dmitry Bagrov ^{1,*}

¹ Faculty of Biology, Lomonosov Moscow State University, 119234 Moscow, Russia; aitsana.dokrunova@gmail.com (A.M.); kaprusakov@gmail.com (K.P.); sidorova.anastasiya.2003@mail.ru (A.S.); a.ramonova@yandex.ru (A.R.)

² Lopukhin Federal Research and Clinical Center of Physical-Chemical Medicine of Federal Medical Biological Agency, 119435 Moscow, Russia; elizaveta.r.pavlova@phystech.edu

* Correspondence: bagrov@mail.bio.msu.ru

Abstract: Electrospun polymer membranes are regarded as prospective biosensor components due to their large specific surface area and diverse opportunities for chemical modifications. However, their intricate porous structure can impede diffusion and render some analyte-binding sites inaccessible. To overcome these diffusion limitations and improve analyte adsorption onto the polymer, a pressure-driven sample flow through the membrane can be employed. To date, the efficiency of pressure-driven analyte delivery into these membranes has not been quantified. Here, we compare forced flow and passive sample diffusion through poly(dioxanone) electrospun membranes. We examine two model analytes, BSA and interleukin-1 beta (IL1b), to address both non-specific and specific binding. Following exposure of the membranes to the test solutions, we measured the residual concentrations of the analytes using fluorometry and enzyme-linked immunosorbent assay (ELISA) techniques. The pressure-driven sample loading was superior to passive diffusion, with a 2.8–11.5-fold change for physical adsorption and a 2.4–3.4-fold difference for specific binding. Our data can be useful for the development of immunoassays and microfluidic devices.

Keywords: electrospun membrane; adsorption; biosensor; analyte; pressure-driven sample flow



check for updates

Citation: Maslakova, A.; Prusakov, K.; Sidorova, A.; Pavlova, E.; Ramonova, A.; Bagrov, D.

Pressure-Driven Sample Flow through an Electrospun Membrane Increases the Analyte Adsorption. *Micro* **2023**, *3*, 566–577. <https://doi.org/10.3390/micro3020038>

Academic Editors: Xi Yao, Yung-Fu Chang and Ming-Liang He

Received: 7 March 2023

Revised: 30 April 2023

Accepted: 19 May 2023

Published: 26 May 2023



Copyright: © 2023 by the authors. Licensee MDPI, Basel, Switzerland. This article is an open access article distributed under the terms and conditions of the Creative Commons Attribution (CC BY) license (<https://creativecommons.org/licenses/by/4.0/>).

1. Introduction

Porous substrates are successfully used in many modern biosensors and analytical techniques such as western blotting, lateral flow (immunochromatographic), and flow-through assays. The main advantage of porous substrates over flat surfaces is the large specific surface area. It ensures higher loading of the analyte-binding molecules and can help to improve the detection limit and decrease the analysis time.

Electrospun membranes constitute a special class of porous media. Electrospinning is a method to produce polymer fibers with diameters ranging from tens of nanometers to several micrometers via an electric field [1]. The typical diameter of electrospun fibers is 1–2 orders of magnitude smaller than the diameter of the polymer fibers produced using the alternative methods [2,3]. The small diameter of the fibers provides a high specific surface area (typically $\sim 10 \text{ m}^2/\text{g}$ [4,5]), making them promising for biosensing applications [6,7].

Numerous studies describe biosensors and analyzers that employ porous substrates. Various methods are used to deliver the sample into the membrane: free diffusion, capillary forces, and forced flow pumping through the membrane. Pressure-driven flow of a sample through a membrane makes it possible to collect the analyte from a relatively large volume and thereby improve the analytical characteristics of the biosensor. Several studies demonstrate the implementation of this approach to collect an analyte from the air using a vacuum cleaner [8,9]. For liquid samples, cyclic pumping through the membrane for gradual depletion of the analyte from the solution also looks promising [10–12]. The

main advantage of using a membrane as the surface for a receptor layer is the increase in the active surface-to-volume ratio. However, the structure of a membrane can impede molecules from accessing the surface deep in the pores. Flow-through pumping addresses these diffusion limitations and effectively updates the analyte concentration within the membrane. In the absence of pumping, the analyte concentration inside the membrane drops due to adsorption. Thus, pumping allows deeper membrane layers to participate in analyte binding.

Although the concept of flow-through pumping seems quite simple at the core, it is tricky in the details. Theoretical analysis of such a flow-based biosensor system must account for all the relevant parameters, including the flow rate, analyte-binding kinetics, sensor geometry, and others [13]. Furthermore, when the binding occurs on the vast surface of pores rather than on a flat substrate, the theoretical analysis becomes incredibly complex. Thus, the optimization of membrane-based biosensors should rely on experimental measurements of their performance. Some studies have demonstrated that pressure-driven sample transport through an electrospun membrane can enhance biosensor performance [10–12]. The enhancement regarded in these studies was a decrease in the analysis time rather than an improvement in detection limit or analyte-binding efficiency. Thus, there is a lack of comparative studies that demonstrate to what extent pressure-driven flow might be superior to simple incubation. In order to fill this gap, we aimed to reveal the quantitative difference between these two sample-loading procedures. Particularly, we focused on the question: “what fraction of the analyte molecules is captured by the membrane in the case of flow and in the case of simple incubation?”. The answer to this question depends not only on the sample-loading procedure but also on the analyte-binding efficiency of the receptor layer. Thus, we regarded two fundamentally different cases—the non-specific binding (physical adsorption, typical $K_d \sim 10^{-4} \text{ M} - 10^{-3} \text{ M}$) and specific binding (antigen–antibody interaction $K_d \sim 10^{-11} \text{ M} - 10^{-9} \text{ M}$, [14]). The two analytes used for these cases were bovine serum albumin (BSA) and interleukin 1 beta (IL1b). We have shown that in both cases, pressure-driven flow ensures higher analyte adsorption than passive diffusion. This feature can be used in the development of membrane-based biosensors and microfluidic devices.

2. Materials and Methods

2.1. Preparation of the Membranes

Electrospun membranes were made of poly(dioxanone) (PDO, BOC Sciences, NY, USA) with an inherent viscosity in the range of 1.55–1.7 dL/g (measured for a 0.8 g/dL solution in HFIP). For electrospinning, a 100 mg/mL solution of PDO in 1,1,1,3,3,3-hexafluoro-2-propanol (HFIP, P&M-Invest, Moscow, Russia) was processed using a TL-Pro-BM Nanofiber Electrospinning Unit (SHENZHEN TONG LI TECH, Shenzhen, China). The distance and voltage between the syringe needle and the collector were 30 cm and 30 kV, respectively. The syringe needle used in these experiments had a 0.7 mm inner and 0.8 mm outer diameter. Polymer solution was supplied using a syringe pump at a rate of 1 mL/h. The thickness of the membranes was in the 60–100 μm range.

2.2. Characterization of the Membranes

The membranes were characterized using scanning electron microscopy (SEM), laser scanning confocal microscopy (LSCM), and IR-spectroscopy. For the SEM imaging, the membranes were covered by a 10 nm gold–palladium alloy layer using Sputter Coater Q150T (Quorum Technologies, Lewes, UK). Imaging was carried out using either TM3000 scanning electron microscope (Hitachi, Japan) or Zeiss Merlin microscope (Zeiss, Oberkochen, Germany). The acceleration voltages were 15 kV and 3 kV, respectively.

For the LSCM imaging, the membranes were treated by fluorescein-labeled antibodies (Roche, Switzerland) for 1 h at 4 °C. Then, the membrane was washed using PBST (PBS with 0.075% Tween-20) for 20 min 3 times. The membranes were embedded into Mowiol 4-88 (Sigma-Aldrich, St. Louis, MO, USA) and stored overnight at 4 °C until the embed-

ding medium dried. Imaging was carried out using an Eclipse Ti-E confocal microscope (Nikon Corporation, Tokyo, Japan) equipped with an A1 confocal module. An Apo TIRF 100×/1.49 objective was used.

The FTIR analysis was performed using the Spectrum Two FT-IR Spectrometer (Perkin-Elmer, Waltham, MA, USA) with the MIRacle ATR unit (PIKE Technologies, Fitchburg, WI, USA). The sample was pressed against a ZnSe prism; the spectra were acquired by accumulating 30 scans.

2.3. Design of the Custom Flow-through Device

We have developed a custom sectional flow chamber for pumping solutions through electrospun membranes (Figure 1A,B). This flow chamber consists of two parts with a piece of membrane clamped between them. To hold all the parts together, an external metal clamp frame was used. The chamber parts were made of polycarbonate sheets with a thickness of 6 mm. Coaxial 0.8 mm holes were drilled through the sheets opposite each other. Metal tubes with the appropriate outside diameter were fixed in the holes with two-component epoxy resin. We created supporting structures on the surface of one of the plates to hold the membrane against the liquid flow. These structures were made from PET-GAG film (laminated sheet made of amorphous polyethylene terephthalate inner layer and polyethylene terephthalate glycol-modified surface layers on both sides) by cutting with a laser engraving machine (Spirit GLS 100 W CO₂) and bonded to the polycarbonate surface using an acrylic film adhesive (3 M 200 MP). On the flow side, the structure was a protruding ring with a diameter of 6 mm to limit the chamber volume above the membrane. On the opposite side, the structure was a supporting grid. These structures served two purposes. First, they prevented the membrane from bending, and second, they ensured an almost uniform flow through the membrane, not just through the central area in front of the metal tube.

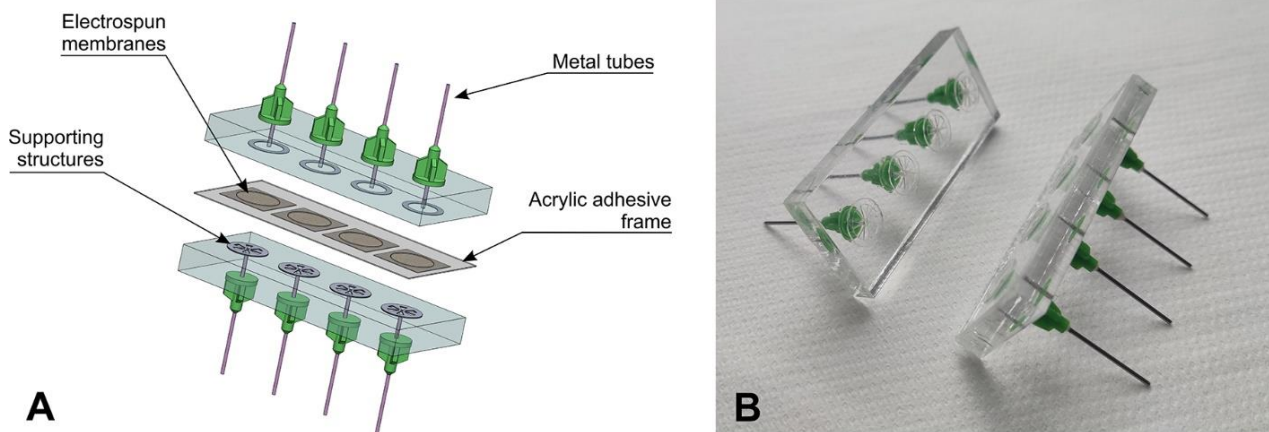


Figure 1. The flow-through chamber for the cyclic pumping of solutions through a membrane. (A) CAD model of the chamber, (B) photo of the chamber.

The pieces of PDO membrane were fixed on a frame of acrylic adhesive and placed into the flow chamber. Then, the flow chamber with the membrane inside it was connected to a peristaltic pump with 0.51 mm silicone pipes via the metal tubes.

2.4. Measurements of the BSA Adsorption

In order to monitor BSA adsorption quantitatively, we labeled 0.5 mg of BSA (Paneco, Moscow, Russia) with the Cy3 fluorophore using the Cy3-NHS reagent (PA13101, Cytiva, Marlborough, MA, USA) at +37 °C for 1 h. The BSA-Cy3 conjugates were purified from the unbound dye by ultrafiltration with a 10 kDa threshold (Amicon Ultra-0.5 Centrifugal Filters, UFC501024, Millipore, Burlington, MA, USA). The resultant molar ratio BSA:dye was estimated as 1:3.

All plastic surfaces (peristaltic pump tubings, microcentrifuge tubes, the 96-well plate) that made contact with the labeled BSA solution were pre-blocked with unlabeled BSA, followed by rigorous washing with PBST (PBS with 0.075% Tween-20) and then with PBS to minimize uncontrolled adsorption of the labeled protein.

BSA-Cy3 at 125, 250, 500, and 1000 ng/mL concentration in PBS was either loaded for incubation (on a shaking platform at 200 rpm) or pumped through the PDO electrospun membranes in a cyclic manner. In either case, the contact between the BSA-Cy3 solution and the membranes lasted 1 h. The setup was kept in the dark to prevent the fluorophore from bleaching. Upon adsorption, the concentration of BSA-Cy3 in the solutions was estimated by comparison of the fluorescence intensity against a calibration prepared from the stock solution. The calibration points were in a range of 62.5–1000 ng/mL of BSA-Cy3 with a double-dilution step. The fluorescence of the BSA-Cy3 solutions was measured using CLARIOstar multifunctional plate reader (BMG LABTECH, Ortenberg, Germany) equipped with a xenon lamp (Supplementary Materials, Figure S1). Fluorescence was excited at a center wavelength of 530 nm (using a 530/20 nm filter), and emission was detected at 580 nm (using a 580/30 nm filter). Similarly, we measured the fluorescence of the membranes.

2.5. Measurements of IL1b Binding

We adopted a commercial IL1b ELISA kit (PSA563Hu01, Cloud-Clone Corp, Wuhan, China) to measure IL1b specific binding onto the electrospun membrane support. Pumping tubings were pre-blocked with 1.5% BSA in PBS for 30 min and then washed with PBST and PBS before membrane loading. Then, the tubes were dried by blowing air, the membranes were fixed, and 350 μ L of the capture antibodies solution at 4 μ g/mL in PBS was loaded by the cyclic pumping through the membranes for 1 h. The capture antibodies were deposited onto the membranes using the flow-through device for both modes of subsequent analyte loading. This was done to maximize the amount of adsorbed antibodies. After capture antibodies' immobilization, the membranes were blocked by a 1.5% BSA solution in PBS by cyclic pumping for 30 min, followed by PBST and PBS washing for 15 min.

Lyophilized IL1b standard (Cloud-Clone Corp, China) was equilibrated to room temperature and reconstituted in a blocking buffer (4% charcoal-dextran-treated fetal bovine serum, 0.1% BSA, PBST) to obtain IL1b stock solution at 1000 pg/mL under mild shaking for 10 min. The IL1b concentrations used for the experiment were 0, 100, 200, and 400 pg/mL. With the "flow-through" setup, they were slightly lower (0, 91, 182, and 364 pg/mL) because the solutions were loaded into the tubings pre-filled with a buffer and became diluted. The solutions were either incubated (on a shaking platform at 200 rpm) or cyclically pumped through the membranes for 1 h. The residual IL1b concentrations after the pumping or incubation were determined by the same IL1b ELISA assay according to the manufacturer's instructions, where the calibration points were prepared from the same IL1b stock solution.

At the washing step, the membranes were washed by PBST; for incubation, washings were performed 3 times with 500 μ L \times 5 min each, so that the overall washing duration time and wash buffer volume were equal to that for pumping (15 min, 100 μ L/min). Then, 350 μ L of biotinylated detection antibodies at 500 ng/mL in the blocking buffer were either incubated or loaded by cyclic pumping for 45 min, followed by washing. To capture the fluorescent or chemiluminescent (CL) signal from the membranes, they were treated by either streptavidin–Alexa Fluor 594 or streptavidin–HRP.

For fluorescence detection, the membranes were treated with 350 μ L of 4 μ g/mL streptavidin–Alexa Fluor 594 solution in the blocking buffer for 30 min (either by incubation or by cyclic pumping). The membrane fluorescence was measured using CLARIOstar multifunctional plate reader (BMG LABTECH, Germany) equipped with a xenon lamp. Fluorescence was excited at a center wavelength of 575 nm (using a 575/20 nm filter), and emission was detected at 630 nm (using a 630/40 nm filter). For the CL detection, streptavidin–HRP was incubated with the membranes for 30 min (the streptavidin–HRP

reagent provided in the ELISA kit was used at 1:100 dilution, as suggested by the manufacturer). The membranes were rigorously washed 5 times for 5 min in PBST and then 2 times for 5 min in PBS. Then, 20 μL of HRP–substrate solution (Clarity Western ECL Substrate, 1705060, Bio-Rad, Hercules, CA, USA) was dropped onto each membrane put on the clean glass and incubated for 5 min. The membranes were scanned using the ChemiDoc XRS+ (Bio-Rad, Hercules, CA, USA) system.

3. Results and Discussion

3.1. Concept of the Experiment

The capture of an analyte from a solution onto a solid medium is controlled by two factors: the analyte diffusion towards the surface and the adsorption kinetics [13]. A porous medium ensures a vast area available for the adsorption; however, the diffusion limitations can become significant. We compared two distinct methods for capturing analytes from the solution onto the membranes: incubation and flow-through cyclic pumping (Figure 2A). The fundamental difference between the two alternatives is the way the analyte is delivered inside the membrane's pores. In the case of incubation without flow-through pumping, the analyte molecules penetrate into the pores only by diffusion. As a result, only the outer layers of fibers participate in capturing the analyte. In contrast, pressure-driven flow refreshes the liquid inside the membrane and ensures a uniform concentration of the analyte throughout the entire pore volume. Consequently, more layers of fibers participate in the analyte-binding reaction, and we expect that more analyte molecules will be captured. To quantify the difference between these cases, we calculated the ratio of the fraction of the bound analyte. It was calculated as follows:

$$\sigma = \frac{C_0 - C_f}{C_0} * 100\% \quad (1)$$

where C_0 is the initial analyte concentration and C_f is the final analyte concentration after incubation or flow-through pumping.

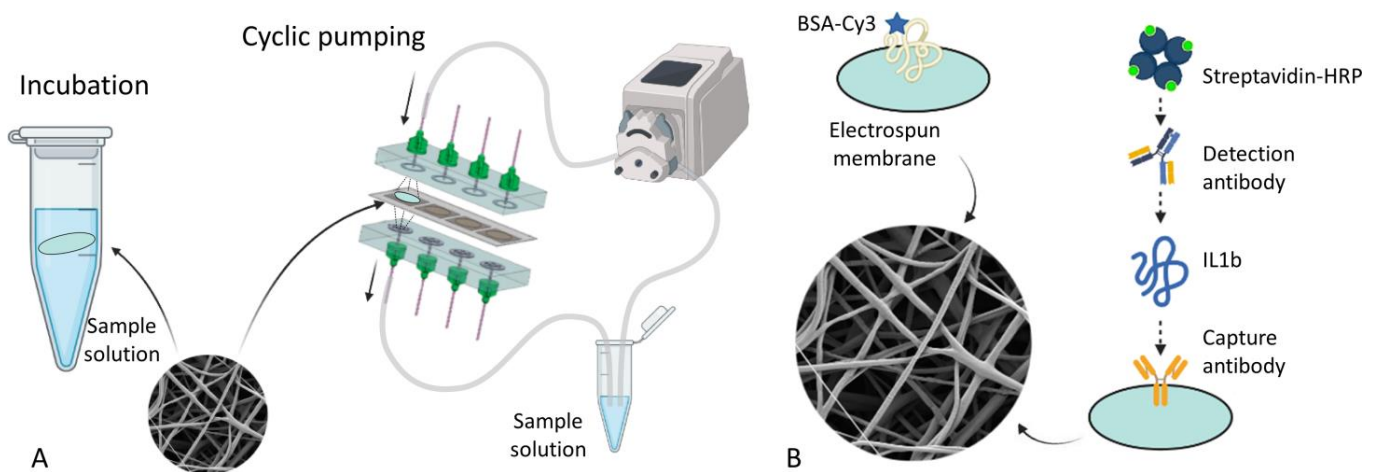


Figure 2. The overall design of the experiment. (A) the schemes of incubation and cyclic pumping, (B) the schemes of adsorption and specific binding.

At the molecular level, we regarded two binding mechanisms—passive adsorption of the molecules onto the membranes and affine binding (Figure 2B). In the former case, adsorption occurs directly on the bare polymer, and in the latter case, it occurs on the polymer pre-treated by the monoclonal antibodies against the analyte. They are also different from the perspective of the concentration measurement procedures (finding C_0 and C_f), as described in the corresponding sections.

3.2. Membrane Characterization

We used polydioxanone (PDO) as the material for the membrane fabrication. The PDO membranes exhibited typical fibrous morphology, as proved by SEM (Figure 3A,B) and LSCM images (Figure 3C). The mean diameter of the fibers was 460 ± 260 nm (mean \pm SD, Figure 3D). Electrospun PDO membranes readily absorb water, and this property ensures that all the fibers participate in the interaction with the analytes, not only the surface layers. The high hydrophilicity of electrospun PDO makes it different from most other polyesters, such as PLA [15] and PCL [16]. Furthermore, PDO, especially within this range of fiber diameters, exhibits a preferential adsorption of BSA and IgG over other serum proteins [17].

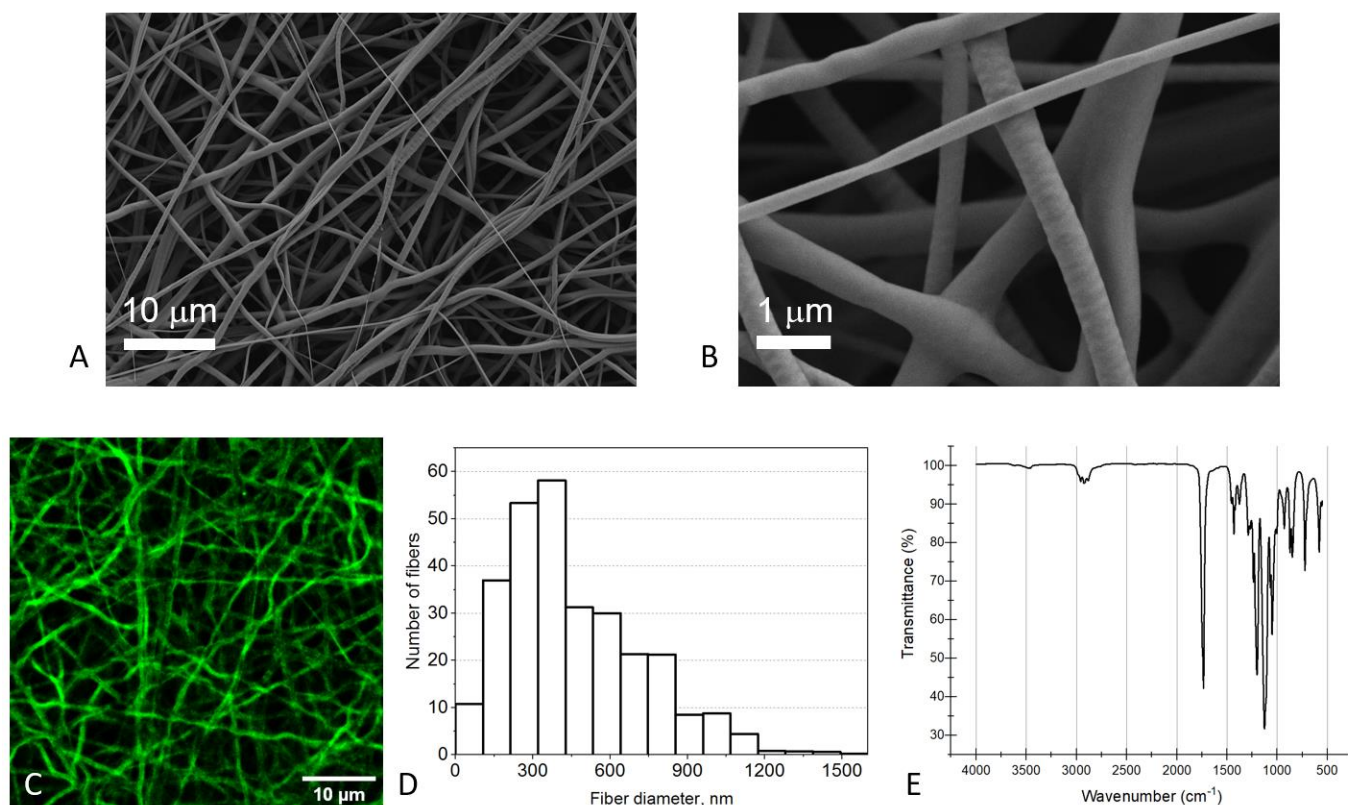


Figure 3. Characterization of the electrospun PDO membranes. (A,B) SEM images, (C) LSCM image (the contrast was enhanced for clarity), (D) distribution of the fiber diameters, obtained by processing eight SEM images, (E) IR spectrum.

The porosity (the fraction of the pore volume) of the PDO membranes was estimated using the LSCM images. It was found to be $68 \pm 2\%$, which seems reasonable for an electrospun membrane [18].

The IR spectrum of the obtained electrospun membranes was in perfect agreement with the spectrum of PDO [19]. The adsorption band at $2850\text{--}3000$ cm^{-1} results from both symmetric and asymmetric stretching vibrations in $\text{--CH}_2\text{--}$ groups. The 1734 cm^{-1} peak corresponds to C=O stretching vibrations, and the 1431 cm^{-1} peak is attributed to bending vibrations of $\text{--CH}_2\text{--}$ groups. The peaks at 1269 cm^{-1} and 1051 cm^{-1} show the C--O stretching vibrations. The peaks near $1060\text{--}1220$ cm^{-1} and $840\text{--}940$ cm^{-1} regions correspond to the C--O--C asymmetric and symmetric stretching vibrations, respectively (Supplementary Materials, Table S1) [19–21].

3.3. Measurements of Non-Specific Adsorption

BSA is a widely used model protein in pure research due to its abundance and cost-effectiveness, high solubility, stability, and well-characterized properties. Its excellent non-specific binding properties with a wide range of surfaces make it a perfect choice for

our study of the non-specific protein adsorption onto the PDO membranes [22]. When a protein solution is cyclically pumped through a membrane, the protein adsorption is higher than in the case of ordinary incubation of a similar membrane in the same solution. This is demonstrated in Figure 4A. For every tested concentration, the fraction of BSA-Cy3 deposited onto the membrane was 2.8–11.5 higher in the case of flow-through deposition than in the case of incubation (the raw data for solution fluorescence are provided in the Supplementary Materials, Figure S2). The difference indicates that the adsorption is mainly limited by protein diffusion in solution rather than the availability of the binding sites on the surface of the fibers. Particularly, the binding sites inside the pores might be more accessible in the “flow-through” rather than the “incubation” setup.

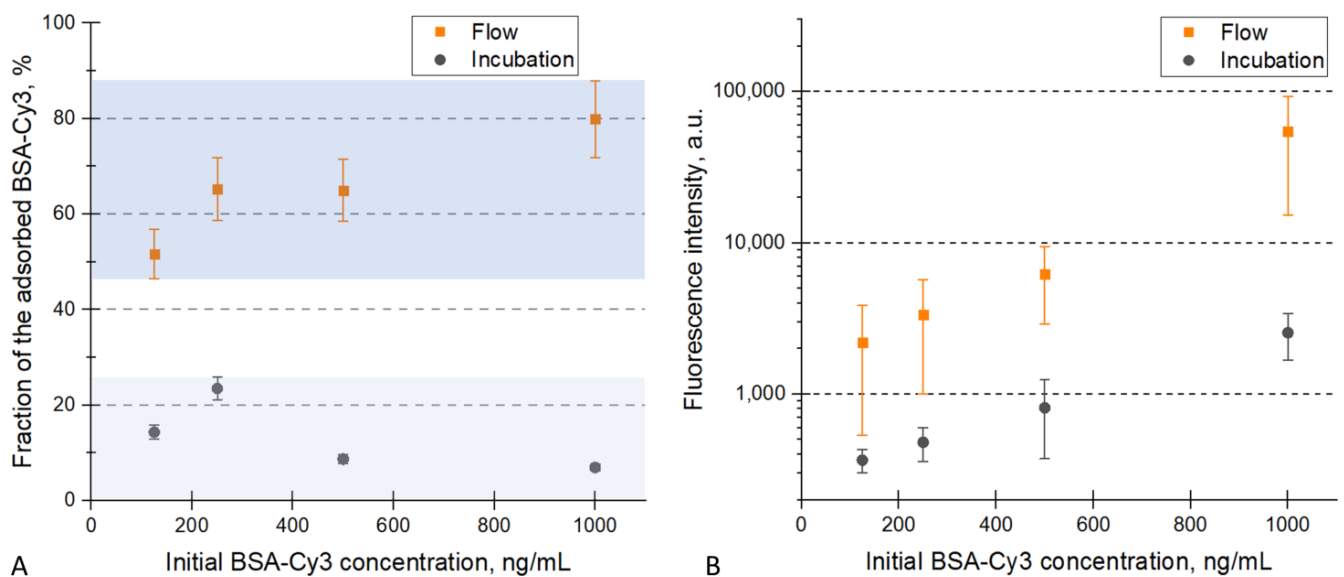


Figure 4. Interaction of BSA-Cy3 with the PDO membranes (comparison of the flow-through system and incubation). (A) the fraction of the adsorbed BSA-Cy3 measured by the solution fluorescence. The two highlighted zones correspond to the two sample deposition procedures. (B) the mean fluorescence signals of the PDO membranes treated by the BSA-Cy3 solutions. The error bars correspond to the standard deviations.

The intense adsorption of BSA-Cy3 onto the PDO membranes could also be monitored by measurements of the membrane fluorescence. The more labeled protein adsorbed onto a membrane, the higher the fluorescence measured. Figure 4B shows that cyclic pumping of the solution through the membrane caused higher protein adsorption than the ordinary incubation. A similar dose-dependency of the fluorescent signals was described for several other biosensors based on electrospun membranes [23,24] or individual electrospun fibers suspended in a liquid [25].

When a solution is used for cyclic pumping through a membrane, it undergoes contact with the inner surface of the tubings. Generally, adsorption can occur not only on the membrane but also on other surfaces, such as tubings. In the control experiments, we have shown that this effect was negligible for the tubings blocked with the non-labeled BSA. We performed a flow-pumping experiment similar to the one described above but without a membrane in the flow chamber. In such an “empty” system, the difference between the resulting BSA-Cy3 concentration and the initial one was within the measurement error. Thus, we concluded that the drop in analyte concentration after pumping through the membrane occurred due to the adsorption onto the membrane rather than the tubing.

In the current section, we describe experiments with BSA-Cy3 fluorophore covalent conjugates rather than bare BSA protein, which helped to measure its concentration directly (we observed a linear concentration–fluorescence dependence within the studied

concentration range). A similar approach is commonly used in studies on adsorption and microfluidics design [26–28].

An electrospun membrane can serve as an efficient sieve (filter) to remove micron-sized particles from water [29,30]. Electrospun membranes can also serve as a separational sieve for biological objects, such as bacteria and yeasts [31]. However, nanometer-sized objects, such as protein molecules, easily penetrate through membranes [32]. The surface pores have a typical size of $\sim 1 \mu\text{m}$ (Figure 3A–C), which is far larger than the hydrodynamic diameter of a BSA molecule (less than 10 nm). Thus, for the protein molecules, the PDO membrane functions as a sorbent rather than a sieve.

3.4. Measurements of Specific Binding

In our experiments on specific binding, the analyte was IL1b, a pro-inflammatory cytokine involved in the pathogenesis of several diseases, such as rheumatoid arthritis, inflammatory bowel disease, and certain autoimmune disorders [33]. Improved biosensors for IL1b can help to monitor its concentration and enable prompt diagnosis and treatment of these conditions.

Specific binding of an analyte requires coating the substrate with high-affinity molecules. The monoclonal anti-IL1b antibodies were deposited onto the PDO membranes using cyclic pumping rather than incubation, as it demonstrated superior adsorption efficiency. Then, the membranes were blocked with BSA and divided into two groups—they were used to capture IL1b by incubation or cyclic pumping. Finally, the IL1b solutions after the binding were analyzed for residual amounts of IL1b. This was carried out using ELISA on a 96-well plate (a typical calibration curve is shown in the Supplementary Materials, Figure S3); the fraction of the bound IL1b was calculated for every membrane. The results are shown in Figure 5. The fraction of the captured IL1b was 2.4–3.4-fold higher if the sample was pumped through a membrane. Because the capture antibodies were deposited equally (by cyclic pumping), the observed difference is attributed to the overall efficiency of analyte capture rather than the amount of immobilized antibodies.

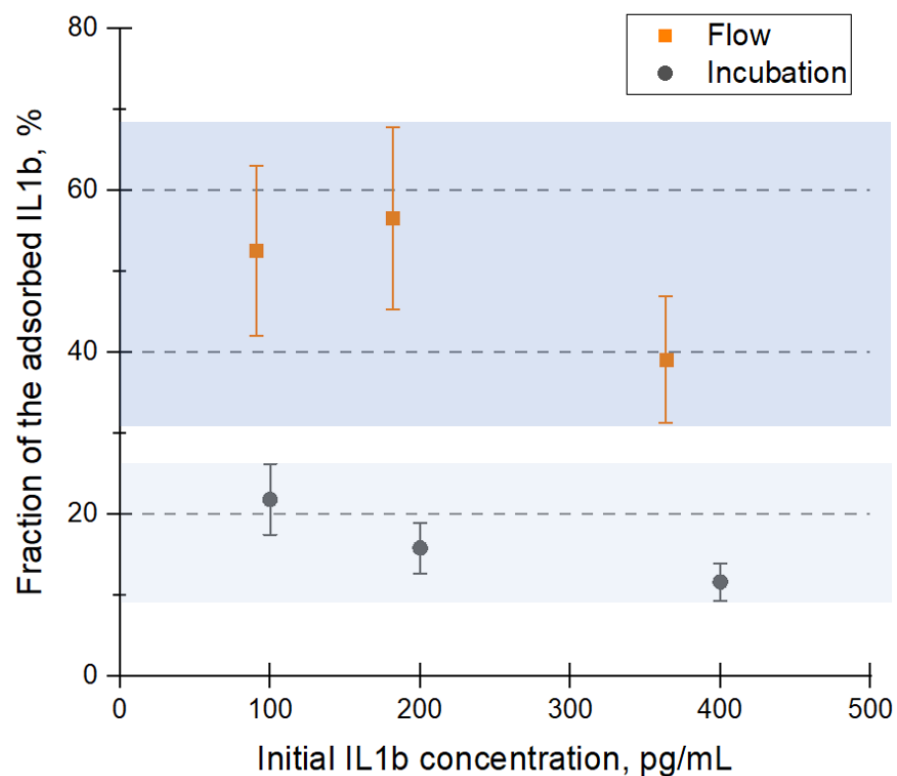


Figure 5. Specific binding of IL1b to the immobilized capture antibodies. The amounts of IL1b were measured using ELISA. The two highlighted zones correspond to the two sample deposition procedures.

Further, we checked which detection method could validate the presence of adsorbed IL1b on the membranes. For this, we treated the membranes with biotin-conjugated detection antibodies. Then, we added streptavidin labeled with either the Alexa Fluor-594 fluorophore or the horseradish peroxidase for fluorescence or CL detection, respectively. In the first case, fluorescence from membranes hardly showed any concentration dependence but rather reflected membrane-to-membrane variability (Figure 6A). We suggest that fluorescent detection was insensitive due to the low analyte concentration; this was different in the case of BSA-Cy3 adsorption, which occurred at higher concentrations and demonstrated a clear concentration dependence (Figure 4B). In the second case, CL turned out to be more sensitive and allowed us to observe the IL1b concentration dependence in both flow and incubation procedures (Figure 6B,C). The pressure-driven flow resulted in higher CL signals than incubation. Thus, if the analyte is at low concentrations, CL detection using sensitive substrate buffers seems more appropriate than fluorescent detection. This result is surprising, because fluorescence detection often is preferable over CL in terms of signal linearity and sensitivity [34,35]. The reasons for this discrepancy could be the non-optimal conditions of membrane treatment with fluorescently labeled streptavidin (e.g., non-optimal concentration and treatment time) or low IL1b concentration.

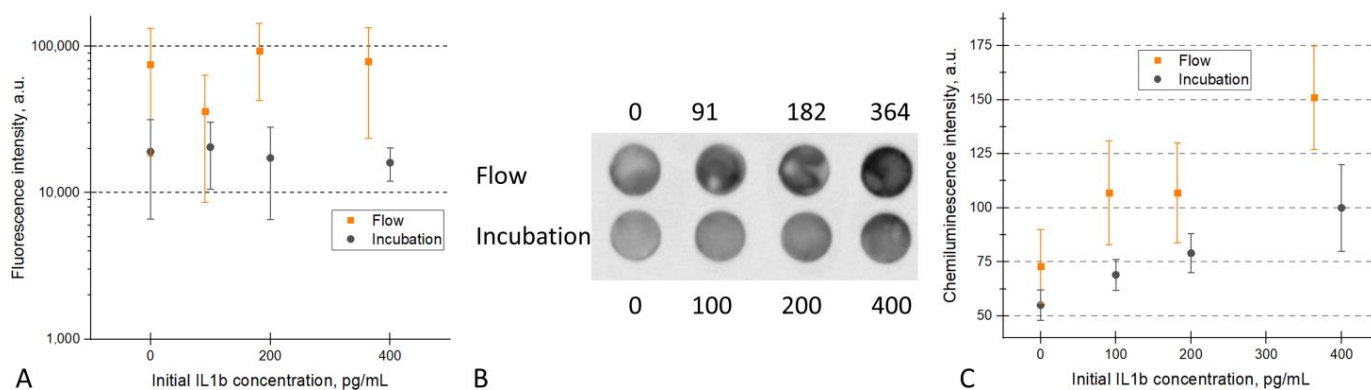


Figure 6. Testing fluorescent and CL detection of specifically bound IL1b on PDO membranes pre-coated with the capture antibodies. After IL1b binding, the membranes were treated with biotinylated detection antibodies. (A) membrane fluorescence intensity upon addition of streptavidin–Alexa Fluor-594. (B) the CL signal scan upon addition of streptavidin–HRP and the ECL substrate. (C) densitometric quantification of the CL signal.

In the experiments on IL1b binding, the capture antibodies were immobilized on PDO using physical adsorption. In many cases, the biosensor efficiency can be improved by chemical coupling of the antibodies to the surface using glutaraldehyde, NHS/EDC, and other reagents [36,37]. Presumably, such modification, in line with the selection of the polymer, can further improve the sensitivity and detection limit of the CL assay conducted on the membrane surface (Figure 6C).

Just as in the case of physical adsorption, in the specific binding case, the analyte capture can be increased by the cyclic pumping of the sample through the membrane. In both cases, it seems to be the consequence of the liquid flow that effectively delivers the analyte molecules into the internal volume of the membrane. In general, regardless of the binding mechanism, the analyte-binding efficiency depends on the flow rate [13]. The optimal flow rate depends on the membrane size and pore geometry, the sample viscosity, and other factors, so its selection requires further research.

4. Conclusions

When electrospun membranes are used as components of biosensors, they provide an extensive area for the immobilization of antibodies and other biomolecules [6]. However, the porous structure of a membrane hinders diffusion of the analyte molecules into the inner layers of the membrane. The penetration of liquid into the pores can be facilitated

by pumping the solution through the membrane. We have shown that pressure-driven sample flow increases protein adsorption. This effect was observed for both non-specific and specific binding, with BSA and IL1b as the analytes, respectively.

Our findings pave the way for further analysis of the diffusion and adsorption processes in electrospun membranes and may serve as a guide for sensor development. Theoretical and experimental optimization of the sample deposition under flow can provide enhancements in terms of detection limit, dynamic range, and analysis time. This requires a detailed analysis of diffusion–adsorption processes on the membrane surface (selection of the polymer, its structure, and surface chemistry modifications) and optimization of the flow conditions (flow rate, cell geometry). In the experiments described above, we kept the sample volume constant for both incubation and cyclic pumping. However, we can easily increase the volume and deliver it to the membrane using the pump. This approach can help us to capture individual analyte molecules from a relatively large sample volume and thus improve the assay sensitivity. Checking this hypothesis, in line with the optimization of the flow conditions, will be the subject of future research. We believe that our approach can be applied to other membranes and biochemical systems.

Supplementary Materials: The following supporting information can be downloaded at <https://www.mdpi.com/article/10.3390/micro3020038/s1>. Figure S1: A typical calibration curve obtained in the experiment on the adsorption of BSA onto the PDO membranes; Figure S2: Concentrations of BSA after the adsorption onto the PDO membranes; Figure S3: A typical calibration curve used to measure the concentration of IL1b after the adsorption; Table S1: The list of peaks in the FTIR spectrum of PDO.

Author Contributions: Conceptualization—A.M., K.P. and D.B., investigation—all authors, formal analysis—A.M., D.B. and A.R., visualization—A.S. and D.B., writing the manuscript—A.M., K.P. and D.B. All authors have read and agreed to the published version of the manuscript.

Funding: This work was supported by the Russian Science Foundation, project No.21-74-10042.

Institutional Review Board Statement: Not applicable.

Informed Consent Statement: Not applicable.

Data Availability Statement: Raw experimental data are available from the authors on demand.

Acknowledgments: Some SEM measurements were performed using the equipment purchased on account of the Lomonosov MSU Development Program. The authors thank Polina Petrova for technical assistance.

Conflicts of Interest: The authors declare no conflict of interest.

References

1. Khan, W.S.; Asmatulu, R.; Ceylan, M.; Jabbarnia, A. Recent progress on conventional and non-conventional electrospinning processes. *Fibers Polym.* **2013**, *14*, 1235–1247. [[CrossRef](#)]
2. Singha, K.; Maity, S.; Singha, M.; Paul, P.; Gon, D.P. Effects of Fiber Diameter Distribution of Nonwoven Fabrics on its Properties. *Int. J. Text. Sci.* **2012**, *1*, 7–14.
3. Luo, C.J.; Stoyanov, S.D.; Stride, E.; Pelan, E.; Edirisinghe, M. Electrospinning versus fibre production methods: From specifics to technological convergence. *Chem. Soc. Rev.* **2012**, *41*, 4708–4735. [[CrossRef](#)]
4. Širc, J.; Hobzova, R.; Kostina, N.; Munzarová, M.; Jukličková, M.; Lhotka, M.; Kubinová, Š.; Zajícová, A.; Michálek, J. Morphological characterization of nanofibers: Methods and application in practice. *J. Nanomater.* **2012**, *2012*, 1–14. [[CrossRef](#)]
5. Omollo, E.; Zhang, C.; Mwasiagi, J.I.; Ncube, S. Electrospinning cellulose acetate nanofibers and a study of their possible use in high-efficiency filtration. *J. Ind. Text.* **2016**, *45*, 716–729. [[CrossRef](#)]
6. Pavlova, E.; Maslakova, A.; Prusakov, K.; Bagrov, D. Optical sensors based on electrospun membranes—Principles, applications, and prospects for chemistry and biology. *New J. Chem.* **2022**, *46*, 8356–8380. [[CrossRef](#)]
7. Asmatulu, R.; Veisi, Z.; Uddin, M.N.; Mahapatro, A. Highly Sensitive and Reliable Electrospun Polyaniline Nanofiber Based Biosensor as a Robust Platform for COX-2 Enzyme Detections. *Fibers Polym.* **2019**, *20*, 966–974. [[CrossRef](#)]
8. Mikheev, A.Y.; Kanev, I.L.; Morozova, T.Y.; Morozov, V.N. Water-soluble filters from ultra-thin polyvinylpyrrolidone nanofibers. *J. Memb. Sci.* **2013**, *448*, 151–159. [[CrossRef](#)]

9. Vladimírsky, M.A.; Shipina, L.K.; Makeeva, E.S.; Alyapkina, Y.S.; Mikheev, A.Y.; Morozov, V.N. Application of water-soluble nanofilters for collection of airborne Mycobacterium tuberculosis DNA in hospital wards. *J. Hosp. Infect.* **2016**, *93*, 100–104. [[CrossRef](#)]
10. Hoy, C.F.O.; Kushiro, K.; Yamaoka, Y.; Ryo, A.; Takai, M. Rapid multiplex microfiber-based immunoassay for anti-MERS-CoV antibody detection. *Sens. Bio-Sens. Res.* **2019**, *26*, 100304. [[CrossRef](#)]
11. Hoy, C.F.O.; Kushiro, K.; Takai, M. Fabrication and assessment of an electrospun polymeric microfiber-based platform under bulk flow conditions with rapid and efficient antigen capture. *Analyst* **2018**, *143*, 865–873. [[CrossRef](#)]
12. Hersey, J.S.; Meller, A.; Grinstaff, M.W. Functionalized Nanofiber Meshes Enhance Immunosorbent Assays. *Anal. Chem.* **2015**, *87*, 11863–11870. [[CrossRef](#)]
13. Squires, T.M.; Messinger, R.J.; Manalis, S.R. Making it stick: Convection, reaction and diffusion in surface-based biosensors. *Nat. Biotechnol.* **2008**, *26*, 417–426. [[CrossRef](#)]
14. Frutiger, A.; Tanno, A.; Hwu, S.; Tiefenauer, R.F.; Vörös, J.; Nakatsuka, N. Nonspecific Binding—Fundamental Concepts and Consequences for Biosensing Applications. *Chem. Rev.* **2021**, *121*, 8095–8160. [[CrossRef](#)]
15. Ke, W.; Li, X.; Miao, M.; Liu, B.; Zhang, X.; Liu, T. Fabrication and Properties of Electrospun and Electrospayed Polyethylene Glycol/Poly(lactic Acid) (PEG/PLA) Films. *Coatings* **2021**, *11*, 790. [[CrossRef](#)]
16. Yew, C.; Azari, P.; Choi, J.; Muhamad, F.; Pingguan-Murphy, B. Electrospun Polycaprolactone Nanofibers as a Reaction Membrane for Lateral Flow Assay. *Polymers* **2018**, *10*, 1387. [[CrossRef](#)]
17. Fetz, A.E.; Fantaziu, C.A.; Smith, R.A.; Radic, M.Z.; Bowlin, G.L. Surface Area to Volume Ratio of Electrospun Polydioxanone Templates Regulates the Adsorption of Soluble Proteins from Human Serum. *Bioengineering* **2019**, *6*, 78. [[CrossRef](#)]
18. Mikhutkin, A.A.; Kamyshinsky, R.A.; Tenchurin, T.K.; Shepelev, D.; Orekhov, A.S.; Grigoriev, T.E.; Mamaguashvili, V.G.; Chvalun, S.N.; Vasiliev, A.L. Towards Tissue Engineering: 3D Study of Polyamide-6 Scaffolds. *Bionanoscience* **2018**, *8*, 511–521. [[CrossRef](#)]
19. Loskot, J.; Jezbera, D.; Bezrouk, A.; Doležal, R.; Andryš, R.; Francová, V.; Miškář, D.; Fučíková, A.M. Raman spectroscopy as a novel method for the characterization of polydioxanone medical stents biodegradation. *Materials* **2021**, *14*, 5462. [[CrossRef](#)]
20. Jin, C.; Liang, B.; Li, J.; Li, F. Biodegradation Behaviors of Poly(p-dioxanone) in Different Environment Media. *J. Polym. Environ.* **2013**, *21*, 1088–1099. [[CrossRef](#)]
21. Zheng, Y.; Zhou, J.; Du, F.; Bao, Y.; Shan, G.; Zhang, L.; Dong, H.; Pan, P. Formation of Mesomorphic Polymorph, Thermal-Induced Phase Transition, and Crystalline Structure-Dependent Degradable and Mechanical Properties of Poly(p-dioxanone). *Cryst. Growth Des.* **2019**, *19*, 166–176. [[CrossRef](#)]
22. Merlot, A.M.; Kalinowski, D.S.; Richardson, D.R. Unraveling the mysteries of serum albumin—More than just a serum protein. *Front. Physiol.* **2014**, *5*, 299. [[CrossRef](#)] [[PubMed](#)]
23. Wang, J.; Kang, Q.S.; Lv, X.G.; Song, J.; Zhan, N.; Dong, W.G.; Huang, W.H. Simple patterned nanofiber scaffolds and its enhanced performance in immunoassay. *PLoS ONE* **2013**, *8*, e82888. [[CrossRef](#)] [[PubMed](#)]
24. Mahmoudifard, M.; Vossoughi, M.; Soleimani, M. Different types of electrospun nanofibers and their effect on microfluidic-based immunoassay. *Polym. Adv. Technol.* **2019**, *30*, 973–982. [[CrossRef](#)]
25. Lee, S.J.; Tatavarty, R.; Gu, M.B. Electrospun polystyrene-poly(styrene-co-maleic anhydride) nanofiber as a new aptasensor platform. *Biosens. Bioelectron.* **2012**, *38*, 302–307. [[CrossRef](#)]
26. Yun, B.J.; Kwon, J.E.; Lee, K.; Koh, W.G. Highly sensitive metal-enhanced fluorescence biosensor prepared on electrospun fibers decorated with silica-coated silver nanoparticles. *Sens. Actuators B Chem.* **2019**, *284*, 140–147. [[CrossRef](#)]
27. Lee, Y.; Lee, H.J.; Son, K.J.; Koh, W.-G. Fabrication of hydrogel-micropatterned nanofibers for highly sensitive microarray-based immunosensors having additional enzyme-based sensing capability. *J. Mater. Chem.* **2011**, *21*, 4476. [[CrossRef](#)]
28. Wu, D.; Han, D.; Steckl, A.J. Immunoassay on Free-Standing Electrospun Membranes. *ACS Appl. Mater. Interfaces* **2010**, *2*, 252–258. [[CrossRef](#)]
29. Gopal, R.; Kaur, S.; Ma, Z.; Chan, C.; Ramakrishna, S.; Matsuura, T. Electrospun nanofibrous filtration membrane. *J. Memb. Sci.* **2006**, *281*, 581–586. [[CrossRef](#)]
30. Aussawasathien, D.; Teerawattananon, C.; Vongachariya, A. Separation of micron to sub-micron particles from water: Electrospun nylon-6 nanofibrous membranes as pre-filters. *J. Memb. Sci.* **2008**, *315*, 11–19. [[CrossRef](#)]
31. Suaste-Gómez, E.; Rodríguez-Roldán, G.; Pérez-Solis, I.; Torres-Huerta, A.; Cruz-Cruz, C.; Tapia-Ramírez, J. Electrospinning Poly(lactic Acid) Polymer Membranes as Biological Sieve for Yeast and Bacteria. *Mater. Sci. Appl.* **2022**, *13*, 389–400.
32. Isik, T.; Demir, M.M. Medical Waste Treatment via Waste Electrospinning of PS. *Fibers Polym.* **2018**, *19*, 767–774. [[CrossRef](#)]
33. Kaneko, N.; Kurata, M.; Yamamoto, T.; Morikawa, S.; Masumoto, J. The role of interleukin-1 in general pathology. *Inflamm. Regen.* **2019**, *39*, 1–16. [[CrossRef](#)]
34. Eaton, S.L.; Hurtado, M.L.; Oldknow, K.J.; Graham, L.C.; Marchant, T.W.; Gillingwater, T.H.; Farquharson, C.; Wishart, T.M. A Guide to Modern Quantitative Fluorescent Western Blotting with Troubleshooting Strategies. *J. Vis. Exp.* **2014**, *93*, e52099. [[CrossRef](#)]
35. Reddig, A.; Roggenbuck, D.; Reinhold, D. Comparison of different immunoassays for γ H2AX quantification. *J. Lab. Precis. Med.* **2018**, *3*, 80. [[CrossRef](#)]

36. Hashemi, S.A.; Bahrani, S.; Mousavi, S.M.; Omidifar, N.; Behbahan, N.G.G.; Arjmand, M.; Lankarani, K.B.; Moghadami, M.; Firoozsani, M. Antibody mounting capability of 1D/2D carbonaceous nanomaterials toward rapid-specific detection of SARS-CoV-2. *Talanta* **2022**, *239*, 123113. [[CrossRef](#)]
37. Hashemi, S.A.; Bahrani, S.; Mousavi, S.M.; Omidifar, N.; Behbahan, N.G.G.; Arjmand, M.; Ramakrishna, S.; Lankarani, K.B.; Moghadami, M.; Shokripour, M.; et al. Ultra-precise label-free nanosensor based on integrated graphene with Au nanostars toward direct detection of IgG antibodies of SARS-CoV-2 in blood. *J. Electroanal. Chem.* **2021**, *894*, 115341. [[CrossRef](#)]

Disclaimer/Publisher's Note: The statements, opinions and data contained in all publications are solely those of the individual author(s) and contributor(s) and not of MDPI and/or the editor(s). MDPI and/or the editor(s) disclaim responsibility for any injury to people or property resulting from any ideas, methods, instructions or products referred to in the content.